

Nucleation Effects on Tip Vortex Cavitation Inception Location

M. T. Khoo^{1,2}, J. A. Venning², B. W. Pearce² and P. A. Brandner²

¹Maritime Division

Defence Science and Technology Group, Fishermans Bend, Victoria, 3207, Australia

²Australian Maritime College

University of Tasmania, Launceston, Tasmania, 7250, Australia

Abstract

Nuclei, or microbubble, populations are inextricably linked to tip vortex cavitation (TVC) inception and dynamics. In order to gain a better quantitative understanding of this relationship, high-speed video measurements were taken in a cavitation tunnel of TVC inception locations about an elliptical hydrofoil in flows with mono- and polydisperse injected nuclei populations. Sample sizes of $O(1000)$ were acquired. For both populations, inception occurred between 0.02 chord lengths upstream of the hydrofoil tip and about 2.1 chord lengths downstream along the cavity trajectory. However, inception location distribution varied significantly with nuclei population. This is explained by the higher concentrations of weaker nuclei in the monodisperse case, which increases the distance along the vortex within which nuclei are susceptible to cavitation. These results provide the foundation for studies on TVC dynamics and acoustics.

Keywords

Tip vortex cavitation; Cavitation nuclei; Bubble dynamics

Introduction

Cavitation inception in practical flows is invariably heterogeneous where nuclei, typically microbubbles, are exposed to a size-dependent critical pressure, resulting in explosive cavity growth. For all but the largest nuclei, critical pressures are well below vapour pressure, or absolute zero, such that liquids typically sustain tensile stresses prior to nuclei activation. A trailing vortex has low pressures in its core, which is the likely location for inception. Nuclei are drawn into the vortex core due to the radial pressure gradient. This phenomenon is known as tip vortex cavitation (TVC), see figure 1. It is often the first type of cavitation to occur about marine propellers and is detrimental to acoustic stealth performance. TVC has been studied extensively [3]. Scale effects due to Reynolds number [17, 21] and nuclei [1, 10] have been the focus of many investigations, with the aim to extrapolate model-scale results to full scale.

Nuclei populations can vary within and between environmental and laboratory waters [14]. They are known to influence TVC behaviour, with earlier onset of cavitation measured in flows with higher concentrations of larger nuclei, also known as ‘weak’ water [1, 10, 13]. While numerous studies of nucleation effects on cavitation have been carried out, only limited observations have been made of their effects on inception location. Such observations have the potential to offer insights into TVC dynamics and acoustics.

The influence of TVC inception location on cavity dynamics and acoustics is of interest as the streamwise variation of the vortex core pressure affects TVC behaviour. The minimum pressure occurs approximately $0.125c$ downstream of the tip for elliptical hydrofoils, where c is the chord length [9, 4]. However, since inception could potentially occur at any location in the flow where the pressure is below vapour pressure, the lo-

cation of inception has been reported anywhere from $0.05c$ upstream to $2c$ downstream of elliptical hydrofoil tips [12, 16, 2].

While it is convenient to describe water as either ‘weak’ or ‘strong’, as done by [2], nuclei populations have size, concentration and spatial distributions and are therefore statistical in nature [22]. This means TVC inception is also statistical and requires large numbers of repeated measurements for accurate characterisation, particularly in nuclei deplete flows [15]. Previous studies using large numbers of cavitation events either span a range of test conditions ([2]: 500 events) or are used for averaging ([18]: 1000 events, [8]: 100 events), and are not used to quantify TVC inception statistics. While it was found that $O(100)$ – $O(1000)$ samples are required to describe the statistics of TVC inception in nuclei deplete flows, it was suggested that fewer samples may be required for flows with higher nuclei populations [15]. A clearer understanding of sample size selection is required to inform the design of TVC inception experiments.

Nuclei populations in cavitation test facilities have been varied by manipulation of the dissolved air content [2, 7] and by microbubble injection [6], the latter enabling more independent control over free and dissolved gases and thus their effects on cavitation behaviour. Even stricter nuclei control and measurement is required to isolate nuclei size and concentration, and to quantify their individual effects on TVC inception location.

In this paper, the effects of two nuclei populations on TVC inception location are presented using large datasets. This provides the basis for studies into TVC dynamics and acoustics, and how they relate to nuclei content and inception location.

Experimental overview

Hydrofoil tip vortex cavitation inception locations were measured in a cavitation tunnel using a high-speed video camera. Two injected nuclei populations were studied at a fixed

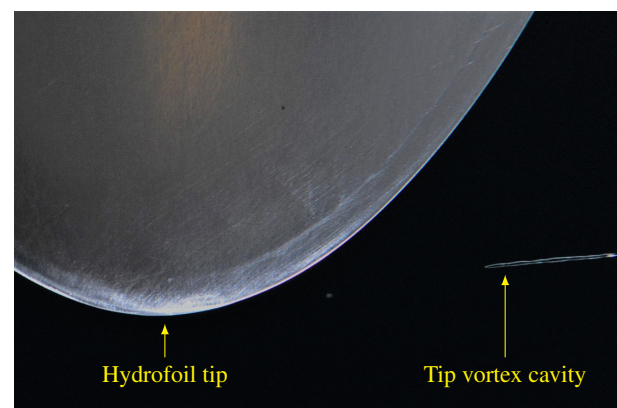


Figure 1. Photograph showing an example of tip vortex cavitation downstream of an elliptical hydrofoil. The flow direction is left to right.

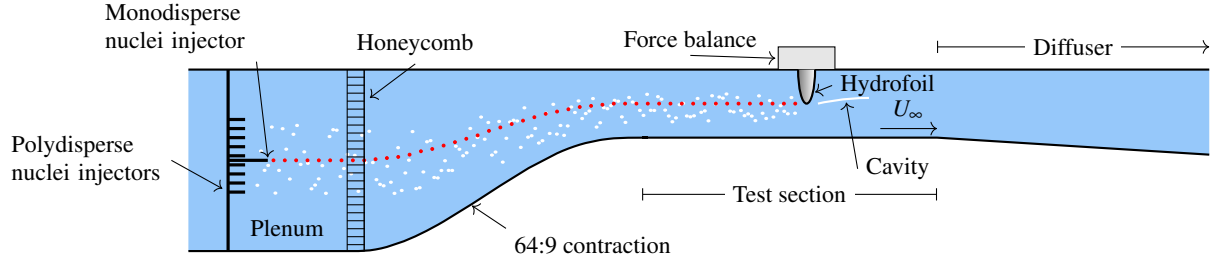


Figure 2. Schematic of the experimental setup in the upper segment of the AMC cavitation tunnel, showing the hydrofoil located in the test section. The force balance allows for angular positioning of the hydrofoil. The test section velocity is U_∞ . Mono- and polydisperse nuclei populations were injected upstream of the test section for different test runs. They are shown as red and white dots, respectively.

Reynolds number and incidence. The experimental setup is shown in figure 2 and further details are provided below.

Test facility

The cavitation tunnel in the Australian Maritime College (AMC) Cavitation Research Laboratory is a medium-sized, variable-pressure water tunnel located in Launceston, Australia. It is constructed of stainless steel (wetted areas) and has a volume of 365 m^3 . The working fluid is demineralised water. The test section cross section is $0.6 \text{ m} \times 0.6 \text{ m}$, with a length of 2.6 m. The test section pressure, p_∞ , can be varied between 4–400 kPa, while the test section velocity, U_∞ , range is nominally 2–12 m/s.

The tunnel design and ancillaries allow for strict control of free and dissolved gas contents. The test flow can be seeded with microbubbles, or nuclei, using injectors mounted in the plenum upstream of the test section. Bubbles are removed downstream of the test section in a large downstream tank (via coalescence and gravity separation) and a lower segment resorber (via extended residence and dissolution). The tunnel features a fast degassing facility, which allows the dissolved gas content to be reduced as required. Further details are provided in [5].

Free and dissolved gas content

Two injected nuclei populations were used for this study. An injected monodisperse microbubble population (hereinafter termed ‘monodisperse’) with a nominal dominant bubble diameter of $100 \mu\text{m}$ was generated using a stainless steel ‘T’-junction with $100 \mu\text{m}$ bore from Valco Instruments Co. Inc. This injector was mounted upstream of the contraction, at the mid-span and mid-height of the plenum, see figure 2.

An injected polydisperse microbubble population (hereinafter termed ‘polydisperse’) with a range of bubble diameters was generated using the cavitation of supersaturated water fed through an array of injectors mounted in the plenum [11, 19]. They are typically arranged in a triangular grid, 80 mm apart (an equivalent spacing of 30 mm in the test section), mounted across three columns of a supporting strut. For this study, only the two outer columns were used to produce a low concentration of polydisperse nuclei, resulting in a spanwise and vertical spacing between injectors of 139 and 80 mm, respectively. This corresponds to 52 and 30 mm in the test section, respectively.

The injected nuclei populations were measured using Mie Scattering Imaging (MSI) [19, 20]. They are presented as histograms of nuclei concentration against bubble diameter in figure 3. The Reynolds number is $Re = \frac{U_\infty c}{\nu}$, where U_∞ is the test section velocity, c is the hydrofoil root chord length and ν is the fluid kinematic viscosity. It was fixed at $Re = 1.5 \times 10^6$ for this study. The cavitation number is $\sigma = \frac{p_\infty - p_v}{\frac{1}{2} \rho U_\infty^2}$, where p_∞ is the

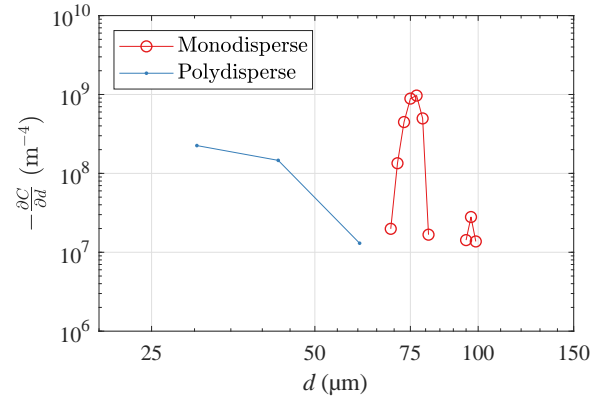


Figure 3. Comparison of nuclei distribution histograms measured using Mie Scattering Imaging ($Re = 1.5 \times 10^6$, $\sigma = 1.6$). The nuclei density distribution, $-\frac{\partial C}{\partial \ln d}$, is plotted against nucleus diameter, d . The monodisperse nuclei distribution features a prominent peak at $d = 77 \mu\text{m}$ and a smaller one at $d = 97 \mu\text{m}$. The polydisperse nuclei distribution has a lower concentration of bubbles across a range of smaller sizes.

freestream pressure in the test section at the same height as the hydrofoil tip, p_v is the vapour pressure and ρ is the fluid density. It was fixed at $\sigma = 1.6$ for this study.

The monodisperse and polydisperse nuclei distributions are constructed from 170 and 15 bubble detections, respectively. While larger sample sizes are preferred, there are sufficient detections to identify the characteristics of each distribution. The monodisperse nuclei distribution exhibits a peak concentration at $d = 77 \mu\text{m}$. A smaller peak at $d = 97 \mu\text{m}$, based on 4 bubble detections, also exists. It is possible that $\sim 97 \mu\text{m}$ diameter bubbles were injected but broke up into $\sim 77 \mu\text{m}$ diameter bubbles. The critical pressure of bubbles in this size range is effectively vapour pressure, which results in weak water.

The polydisperse nuclei distribution comprises a lower concentration of bubbles across a range of smaller diameters. It is stronger than the monodisperse nuclei distribution, as no bubbles larger than about $60 \mu\text{m}$ in diameter were detected.

The dissolved oxygen content was maintained between 2.6 and 3.7 mg/L (i.e. 29–41% relative to saturation at atmospheric pressure) throughout the experiment.

Cavitation inception location measurement and processing

A stainless steel hydrofoil with an elliptical planform and NACA 0012 cross section was studied. It has a root chord length of 150 mm and a span of 300 mm. It was mounted to a six-component force balance with a stepper motor and encoder

for angular positioning. This unit was installed 1.45 m from the test section entrance, as shown in figure 2. The hydrofoil incidence, α , was fixed at 6° throughout this study.

Visual measurements were taken using a high-speed camera (Phantom v2640 with Nikon 24 mm focal length lens, frame rate 16 kHz). It was mounted beneath the test section. LED lighting was used to illuminate the cavities. Recordings were triggered using an image-based trigger.

Visual measurements of a single cavitation event in a flow injected with monodisperse bubbles are shown in figure 4. Image processing was carried out using MATLAB software. The composite photograph (left) shows the different stages of development of a single cavity. Boundaries of the cavity trajectory were identified using an image of a steady cavity attached to the hydrofoil tip. The distance along the cavity trajectory downstream of the hydrofoil tip, s , is normalised by the hydrofoil root chord length, c , in this analysis (i.e. s/c). Note that the image-based trigger used for video acquisition was located at $s/c \approx 2.4$.

Pixels with the maximum intensity within the trajectory bounds at each s/c location were extracted from each video frame. Space-time plots were constructed which quantify cavity development. Intensity and area filters were applied to identify tip vortex cavities. Cavitation inception was defined as the elongation of a captured nucleus, so the filter was tuned to only pass such cavities. The downstream distance along the cavity trajectory corresponding to the earliest appearance of the cavity (i.e. the top of the leftmost point of the shaded region in figure 4) was defined as the inception location, s_i/c .

Results and Discussion

Histograms of inception location are provided in figure 5. A total of 4023 events were captured for the monodisperse case and 1405 for the polydisperse. Although $O(1000)$ events were recorded in each case, the inception location distributions converge to that of the final dataset within $O(100)$ events.

The inception location distributions differ significantly. In the monodisperse case, a greater proportion of inception events occur at downstream locations. The higher concentration of weaker nuclei in the monodisperse case increases the distance along the vortex within which nuclei are susceptible to cavitation. The distribution is relatively uniform between $s_i/c = 0$ and 0.6. This could be associated with a stronger radial pressure gradient across this range, which draws larger bubbles into low pressure regions faster than smaller ones. It may be that $p \ll p_v$ in this region, but such inferences are made with caution as vaporous and gaseous cavitation have not been distinguished in this study. The former occurs when the equilibrium of a nucleus becomes unstable when exposed to its critical pressure, resulting in explosive growth as the cavity fills with vapour. The latter occurs when a larger bubble grows due to pressure reduction and gaseous diffusion at a pressure higher than vapour pressure. Measurement or simulation of the pressure field could assist with understanding the physics of nuclei capture and type of cavitation that occurs.

For the polydisperse case, inception events most commonly occur just downstream of the tip, tending to decrease in probability with increasing downstream distance. The ‘window of opportunity’ for inception for this case is smaller due the presence of stronger nuclei that require higher tensions to activate, hence a greater clustering of data points about what is presumably the location of minimum vortex pressure. The location of the peak shows agreement with the location of minimum pressure in the tip vortex of an elliptical hydrofoil, which has been found to be $0.125c$ downstream of the tip [9, 4].

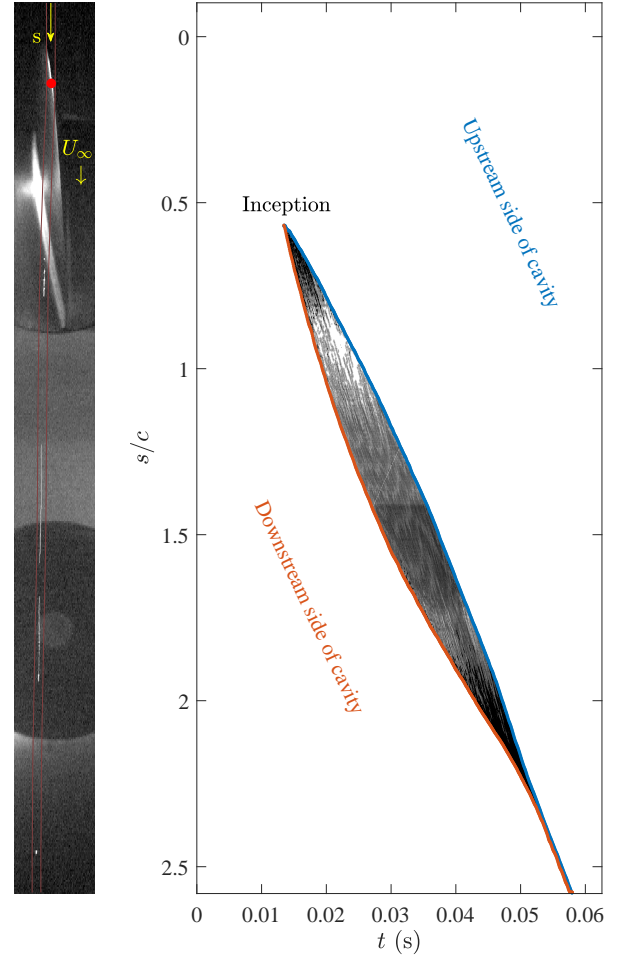


Figure 4. Visual measurements of a single cavitation event in a flow injected with monodisperse bubbles ($Re = 1.5 \times 10^6$, $\sigma = 1.6$, $\alpha = 6^\circ$). The composite photograph (left) shows different stages of cavity development, with the flow direction top to bottom. The hydrofoil tip is marked with a red circle. The distance along the cavity trajectory (bounded by the dark red lines) downstream of the tip, s , normalised by the root chord length, c , is plotted against time, t , in the space-time graph (right). The shaded region corresponds to a cavity identified using intensity and area filters. The inception location is at $s_i/c = 0.58$.

For both nuclei populations, inception events were detected up to $0.02c$ upstream of the tip. This is indicative of the start of tip vortex development in this region. Inception events were also detected up to $s_i/c \approx 2.1$ for both cases. These results are in agreement with [16] and [12] who observed inception between $0.05c$ upstream and $2c$ downstream of the tip (in the stream-wise direction), respectively. In the present study, some inception events exhibited only minimal elongation. This occurred at $s_i/c \gtrsim 1.2$ for the monodisperse case and $s_i/c \gtrsim 1.8$ for the polydisperse. This indicates weakening of the vortex, but it is unclear whether these inception events constitute vaporous or gaseous cavitation.

Conclusions

Nucleation effects on tip vortex cavitation inception location about an elliptical hydrofoil have been studied in a cavitation tunnel using high-speed video measurements. Sample sizes of $O(1000)$ were acquired. The nuclei population was found to influence inception location distributions significantly. In the monodisperse case, a greater proportion of events occurred at

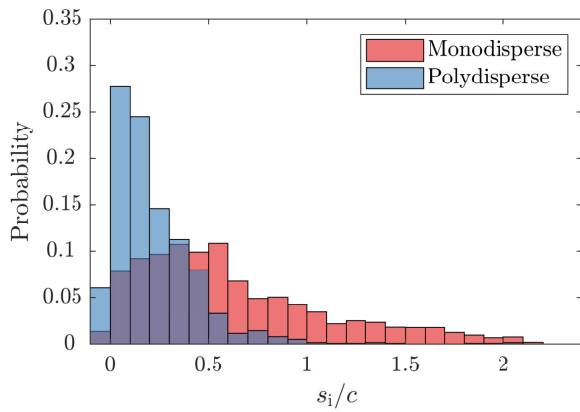


Figure 5. Histograms of inception location, s_i/c , for different nuclei populations ($Re = 1.5 \times 10^6$, $\sigma = 1.6$ and $\alpha = 6^\circ$). The hydrofoil tip corresponds to $s_i/c = 0$. The distribution is more uniform for the monodisperse case, especially between $s_i/c = 0$ and 0.6. Inception is most likely just downstream of the tip for the polydisperse case. Inception events were observed between $s_i/c = -0.02$ and about 2.1 for both cases.

downstream locations. This was attributed to the higher concentration of weaker nuclei in this flow, which increased the distance along the vortex within which nuclei could cavitate. For both nuclei populations, inception was detected between 0.02 chord lengths upstream of the hydrofoil tip and about 2.1 chord lengths downstream of the tip along the cavity trajectory. Some of the inception events exhibited only minimal elongation. The distinction between vaporous and gaseous cavitation should be given further consideration as it would enable the local pressure to be inferred with greater confidence. This study provides the foundation for investigations into TVC acoustics and its dependence on TVC dynamics using cavity properties determined from high-speed video measurements.

Acknowledgements

The authors acknowledge the support of the University of Tasmania and the Defence Science and Technology Group. The authors thank AMC technical officers, Mr Robert Wrigley and Mr Steven Kent for providing technical assistance with test facility configuration and operation.

References

[1] Arndt, R.E.A. and Keller, A.P. (1992) Water quality effects on cavitation inception in a trailing vortex. *J Fluids Eng*, 114(3), 430–438.

[2] Arndt, R.E.A. and Maines, B.H. (2000). Nucleation and bubble dynamics in vortical flows. *Journal of Fluids Engineering - Transactions of the ASME*, 122(3), 488–493.

[3] Arndt, R.E.A. (2002). Cavitation in vortical flows. *Annual Review of Fluid Mechanics*, 34(1), 143–175.

[4] Asnaghi, A., Svennberg, U. and Bensow, R.E. (2020). Large Eddy Simulations of cavitating tip vortex flows. *Ocean Engineering*, 195, 106703.

[5] Brandner, P.A., Lecoffre, Y. and Walker, G.J. (2007). Design considerations in the development of a modern cavitation tunnel. in *Proc. 16th Australasian Fluid Mechanics Conference*, 630–637.

[6] Briançon-Marjollet, L. and Merle, L. (1996). Inception, development and noise of a tip vortex cavitation. in *Proc. 21st Symp on Naval Hydrodynamics*, 851–864.

[7] Chang, N., Ganesh, H., Yakushiji, R. and Ceccio, S.L. (2011). Tip vortex cavitation suppression by active mass injection. *J Fluids Eng*, 133(11), 111301.

[8] Choi, J. and Ceccio, S.L. (2007). Dynamics and noise emission of vortex cavitation bubbles. *J Fluid Mech*, 575, 1–26.

[9] Fruman, D. and Dugue, C. (1994). Tip vortex roll-up and cavitation. in *Proc. 19th Symp on Naval Hydrodynamics*, 633–654.

[10] Gindroz, B. and Billet, M.L. (1998). Influence of the nuclei on the cavitation inception for different types of cavitation on ship propellers. *J Fluids Eng*, 120(1), 171–178.

[11] Giosio, D., Pearce, B.W. and Brandner, P.A. (2016). Influence of pressure on microbubble production rate in a confined turbulent jet. in *Proc. 20th Australasian Fluid Mechanics Conference*, Paper 717.

[12] Higuchi, H., Arndt, R.E.A. and Rogers, M.F. (1989). Characteristics of tip vortex cavitation noise. *J Fluids Eng*, 111, 495–501.

[13] Khoo, M.T., Venning, J.A., Pearce, B.W. and Brandner, P.A. (2018). Nucleation effects on hydrofoil tip vortex cavitation. in *Proc. 21st Australasian Fluid Mechanics Conference*, Paper 592.

[14] Khoo, M.T., Venning, J.A., Pearce, B.W., Takahashi, K., Mori, T. and Brandner, P.A. (2020). Natural nuclei population dynamics in cavitation tunnels *Experiments in Fluids*, 61(2), 34.

[15] Khoo, M.T., Venning, J.A., Pearce, B.W. and Brandner, P.A. (2020). Statistical aspects of tip vortex cavitation inception and desinence in a nuclei deplete flow. *Experiments in Fluids*, 61(6), 145.

[16] Maines, B.H. and Arndt, R.E.A. (1993). Bubble dynamics of cavitation inception in a wing tip vortex *ASME Cavitation and Multiphase Flow Forum, FED*, 1993, 153, 93–97.

[17] McCormick, B.W. (1962). On cavitation produced by a vortex trailing from a lifting surface. *J Basic Eng*, 84(3), 369–378.

[18] Oweis, G.F., Choi, J. and Ceccio, S.L. (2004). Dynamics and noise emission of laser induced cavitation bubbles in a vortical flow field. *The Journal of the Acoustical Society of America*, 115(3), 1049–1058.

[19] Russell, P.S., Barbaca, L., Venning, J.A., Pearce, B.W. and Brandner, P.A. (2020). Measurement of nuclei seeding in hydrodynamic test facilities. *Experiments in Fluids*, 61(3), 1–18.

[20] Russell, P.S., Venning, J.A., Pearce, B.W. and Brandner, P.A. (2020). Calibration of Mie Scattering Imaging for microbubble measurement in hydrodynamic test facilities. *Experiments in Fluids*, 61(4), 1–17.

[21] Shen, Y.T., Jessup, S. and Gowing, S. (2009). Tip vortex cavitation inception scaling for high Reynolds number application. *ASME/JSME 2003 4th Joint Fluids Summer Eng Conf*, 233–239.

[22] Venning, J.A., Khoo, M.T., Pearce, B.W. and Brandner, P.A. (2018). Background nuclei measurements and implications for cavitation inception in hydrodynamic test facilities. *Experiments in Fluids*, 59(4), 71.